Please cite this article in press as: Gao et al., Catalytic strategies and mechanisms for enhancing MgH_2 solid-state hydrogen storage, Chem Catalysis (2026), https://doi.org/10.1016/j.checat.2026.101692

Chem Catalysis

CellPress

Perspective

Catalytic strategies and mechanisms for enhancing MgH_2 solid-state hydrogen storage

Zhengyang Gao,[1,2] Xiaojin Yang,[1,2] Zelong Zhuang,[1,2] Yizhou Zhang,[3] Jianghao Cai,[1,2] Yanxin Li,[1,2] Wenfeng Fu,[1,2] Hao Li,[3,*] and Weijie Yang[1,2,*]

[1]Department of Power Engineering, North China Electric Power University, Baoding, Hebei 071003, China

[2]Hebei Key Laboratory of Energy Storage Technology and Integrated Energy Utilization, North China Electric Power University, Baoding, Hebei 071003, China

[3]Advanced Institute for Materials Research (WPI-AIMR), Tohoku University, Sendai 980–8577, Japan

*Correspondence: li.hao.b8@tohoku.ac.jp (H.L.), yangwj@ncepu.edu.cn (W.Y.)

https://doi.org/10.1016/j.checat.2026.101692

THE BIGGER PICTURE To make hydrogen a truly practical and versatile energy carrier, storage materials must meet stringent targets for capacity, operating temperature, and reversibility while relying on earth-abundant elements. Magnesium hydride (MgH_2) may approach these targets in terms of capacity, but its kinetic bottlenecks remain an Achilles' heel, forcing high operating temperatures and imposing heavy system penalties. Taking the "burst effect" as a starting point, this perspective argues that understanding how catalysts reshape the dehydrogenation process by tuning active phases, enabling multicomponent synergies, and tailoring electronic structure is key to overcoming kinetic limitations in solid-state hydrogen storage. By linking mechanistic insights with design principles and theory-driven and data-driven screening, catalysts can be transformed from empirical additives into rationally designed functional units for future hydrogen storage technologies.

SUMMARY

MgH_2 offers a high gravimetric hydrogen capacity and earth-abundant chemistry, yet its practical deployment is blocked by a high dehydrogenation enthalpy and sluggish surface-controlled kinetics. Recent work has revealed a characteristic "burst effect," in which the first surface dehydrogenation step carries the highest barrier, while subsequent layers desorb much more easily. This perspective takes the burst effect as a unifying lens to examine how catalytic strategies reshape the initial surface step and, through it, the overall hydrogen-release behavior of MgH_2. We summarize recent experimental advances in three major classes of catalysts and relate their performance to evolving atomistic mechanisms. We then discuss emerging theoretical tools, from density functional theory (DFT) calculations to machine learning interatomic potentials and descriptor-based models, that connect surface chemistry to macroscopic kinetics and enable theory-guided catalyst design. Finally, we outline key challenges and opportunities for translating burst-effect-aware design principles into practical Mg-based hydrogen storage systems.

INTRODUCTION

Hydrogen is widely regarded as a key secondary energy carrier for achieving deep decarbonization and the large-scale integration of renewable energy, with promising applications in transportation, stationary energy storage, and the chemical industry.[1,2] However, the lack of efficient, safe, and reversible hydrogen storage technologies remains one of the main bottlenecks in the large-scale deployment of hydrogen as an energy carrier.[3] From a practical perspective, onboard hydrogen storage places stringent requirements on storage materials to enable rapid and controllable hydrogen release at moderate operating temperatures.[4] These requirements impose stringent and interrelated constraints on the hydrogen storage capacity, thermodynamic properties, sorption kinetics, and operating temperature window of candidate storage materials.

Among the various hydrogen storage technologies, solid-state hydrogen storage offers inherent advantages in safety and volumetric hydrogen storage density over high-pressure gaseous and liquid hydrogen storage.[5] Within this category, metal hydrides are considered one of the most promising families of solid-state hydrogen storage materials because they combine

Please cite this article in press as: Gao et al., Catalytic strategies and mechanisms for enhancing MgH_2 solid-state hydrogen storage, Chem Catalysis (2026), https://doi.org/10.1016/j.checat.2026.101692

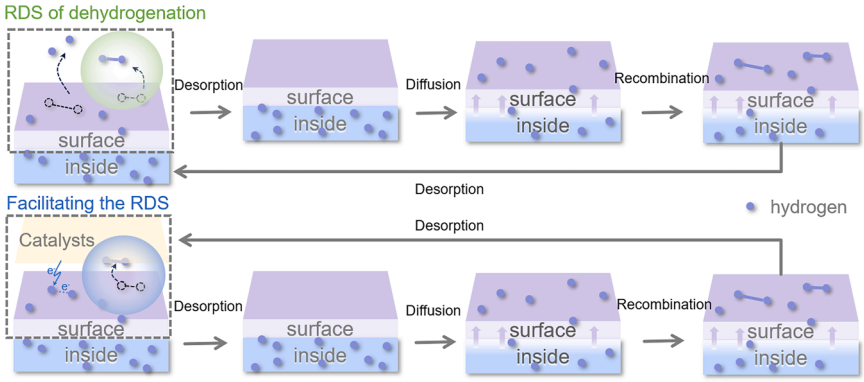

Figure 1. Rate-determining step in MgH_2 dehydrogenation and its surface catalytic promotion

high volumetric hydrogen density with good reversible hydrogen absorption and desorption. At the same time, metal hydrides commonly suffer from several intrinsic limitations, including thermodynamic stability that is either too high or too low, sluggish sorption kinetics, limited practically achievable reversible hydrogen capacity, and inadequate cycling stability.[6,7] MgH_2 is one of the most extensively studied metal hydrides because Mg is abundant and inexpensive and MgH_2 provides a high theoretical gravimetric hydrogen capacity of ~7.6 wt % H_2. Although the gravimetric hydrogen capacity of MgH_2 at the material level is intrinsically high, its dehydrogenation enthalpy is relatively high. As a result, both the equilibrium and the practically relevant desorption temperatures are typically in the range of 300°C–350°C or even higher, and the hydrogen absorption-desorption kinetics are slow. This contrast points to the acceleration of dehydrogenation kinetics as a key requirement for achieving hydrogen release from MgH_2 at more moderate operating temperatures.[8–10]

To overcome the kinetic bottlenecks associated with MgH_2 dehydrogenation, previous studies have primarily focused on several strategies, including nanostructuring[11] (e.g., high-energy ball milling, particle size refinement, and nanoconfinement in porous scaffolds), alloying and elemental doping,[12] and the introduction of catalysts.[13] Among these approaches, catalytic modification has received particular attention. On the one hand, appropriately designed catalysts can markedly reduce the dehydrogenation energy barrier and accelerate hydrogen absorption and desorption even at relatively low catalyst loadings, thereby minimizing the dilution of the reversible hydrogen storage capacity. On the other hand, by constructing favorable interfacial structures and tuning the electronic structure, catalysts can work synergistically with nanostructuring and nanoconfinement to optimize hydrogen diffusion pathways and improve heat and mass transport. Enhancing the dehydrogenation performance of MgH_2 through catalytic strategies is therefore regarded as one of the key routes to overcoming its kinetic limitations.[14–16]

Recent theoretical and experimental studies have revealed that the dehydrogenation of MgH_2 exhibits the so-called "burst effect" (also referred to as the "dam-break effect").[17–19] Within a certain temperature range, desorption of the first surface hydrogen layer is the most kinetically demanding step and is associated with the highest activation barrier along the dehydrogenation pathway. Once this step is overcome, the barriers to desorbing hydrogen from deeper layers decrease substantially. Importantly, across the dehydrogenation pathway, the surface dehydrogenation barriers remain consistently higher than the barriers for hydrogen migration from the bulk toward the surface. Therefore, surface dehydrogenation constitutes the dominant kinetic resistance and can be regarded as the rate-determining step (RDS) across the dehydrogenation process of MgH_2. It also helps rationalize why catalysts that primarily act at the MgH_2 surface can still accelerate the overall kinetics, because they directly target the RDS (Figure 1), which we propose here as a viewpoint distinct from prior MgH_2 catalysis reviews. Accordingly, selective activation and control of the surface dehydrogenation step are critical for improving the overall dehydrogenation performance. This effect leads to a clear design principle: if catalysts can be rationally designed to effectively activate the MgH_2 surface and lower the desorption barrier of the surface hydrogen layer, the kinetic advantages associated with the burst effect can be amplified. In this way, the overall dehydrogenation barrier can be reduced at the microscopic level, and the onset dehydrogenation temperature of MgH_2 can be significantly lowered at the macroscopic level. Catalyst design guided by surface activation and explicitly accounting for the burst effect can therefore be regarded as a targeted modification strategy that is well aligned with the intrinsic dehydrogenation kinetics of MgH_2 and holds considerable promise for both fundamental studies and practical applications. Recent reviews of MgH_2 catalysis have provided comprehensive surveys organized around catalyst compositions, material architectures, or modification strategies, and they typically discuss performance trends using macroscopic kinetic metrics. However, the burst effect has been overlooked as an important factor in mechanistic understanding and catalyst design for MgH_2 dehydrogenation. Current catalyst development still relies largely on empirical screening and repeated trial and error largely due to the lack of sufficiently developed theoretical guidance. Therefore, in this perspective, we revisit prior catalyst design and materials development through the lens of the burst effect.

In this perspective, we use the burst effect as a starting point to explore how catalyst design can be used to fully exploit the intrinsic dehydrogenation potential of Mg-based hydrogen storage materials. We first provide a brief overview of the theoretical and experimental evidence for the burst effect and elucidate its implications for understanding the dehydrogenation kinetics of MgH_2. We then summarize recent progress in representative catalyst systems that improve the dehydrogenation performance of MgH_2 and in the underlying intrinsic and catalyst-assisted dehydrogenation mechanisms. On this mechanistic and computational basis, we further discuss two complementary theory-guided design strategies: direct design of Mg-based materials and catalysts using first-principles calculations and

Please cite this article in press as: Gao et al., Catalytic strategies and mechanisms for enhancing MgH_2 solid-state hydrogen storage, Chem Catalysis (2026), https://doi.org/10.1016/j.checat.2026.101692

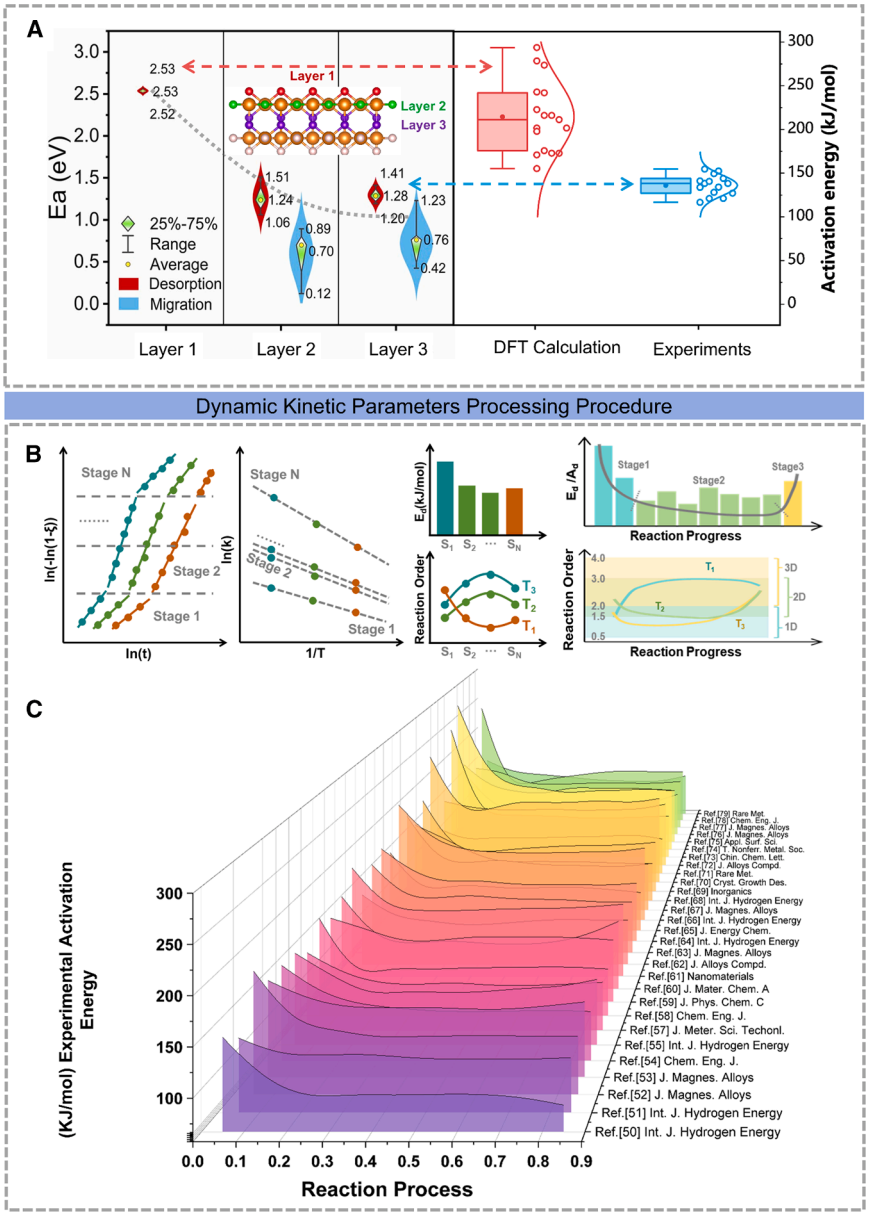

Figure 2. Density functional theory calculations and data-driven methodology for identifying the "burst effect" in MgH_2 dehydrogenation

(A) The three-layer atomic H migration and dehydrogenation energy barriers and statistical distributions of activation energies from theoretical calculations and experimental fittings. Reprinted with permission from Dong et al.[17] Copyright 2022 Royal Society of Chemistry.

(B) Dynamic kinetic parameters processing procedure for Mg-based hydrogen storage materials.

(C) Statistics on dynamic activation energy from experimental curves. Reprinted with permission from Cai et al.[18] Copyright 2025 Elsevier.

descriptor-based approaches that translate computed properties into practical design rules and, where appropriate, into data-driven screening protocols. Finally, we offer several key perspectives and outline future research directions, emphasizing that catalyst design guided by the burst effect may not only advance Mg-based hydrogen storage materials but also provide general concepts and methods for a broader range of solid-state hydrogen storage systems.

THE BURST EFFECT IN DEHYDROGENATION: THEORETICAL AND EXPERIMENTAL EVIDENCE

The burst effect was first identified using first-principles calculations. In 2022, Dong et al.[17] performed a layer-by-layer density functional theory (DFT) analysis of MgH_2(110) dehydrogenation (from layer 1 to layer 3) and summarized the kinetic landscape in Figure 2A. They found that H_2 desorption from the first surface hydrogen layer (layer 1) has a very high barrier of 2.52–2.53 eV, whereas the corresponding barriers for subsequent near-surface layers are substantially lower (e.g., 1.06–1.51 eV for layer 2 and 1.2–1.41 eV for layer 3). Importantly, along the computed pathways, the barriers for hydrogen migration from subsurface layers toward the surface are typically lower than the corresponding surface dehydrogenation barriers, meaning that, even after the initial barrier drops, dehydrogenation from the surface layer still represents the dominant kinetic resistance relative to the hydrogen migration from bulk to surface. Therefore, within this mechanistic picture, the surface dehydrogenation step, especially the removal of the first surface hydrogen layer, can be regarded as the RDS. By combining these results with analyses of Mg-H bond strength and electronic localization, the authors showed that the Mg-H bonds progressively weaken as dehydrogenation proceeds, thereby accelerating subsequent hydrogen migration and desorption. Accordingly, after the initial surface-layer removal, the dominant resistance is expected to relax as the interfacial bonding environment and the near-surface hydrogen-vacancy landscape evolve with reaction progress. This microscopic framework also motivates a discussion based on descriptors, including hydrogen-vacancy formation energetics, changes in the integrated crystal orbital Hamilton population (ICOHP) that quantify Mg-H bond weakening, and catalyst electronic descriptors such as shifts in the d-band center, which can be linked to macroscopic observables. For example, Li et al. developed a descriptor-based, data-driven model for MgH_2 dehydrogenation barriers and showed that the predicted barriers

Please cite this article in press as: Gao et al., Catalytic strategies and mechanisms for enhancing MgH_2 solid-state hydrogen storage, Chem Catalysis (2026), https://doi.org/10.1016/j.checat.2026.101692

are highly consistent with onset dehydrogenation temperatures compiled from representative metal-doped MgH_2 experiments.[20] At the same time, we note that macroscopic metrics such as the onset temperature and peak temperature are composite readouts. In addition to intrinsic changes in surface kinetics, they can be influenced by heating rate, particle size and defect distributions, MgO formation and oxidation state evolution, and catalyst dispersion that changes the effective interfacial contact. Therefore, shifts in the onset temperature and peak temperature should be interpreted together with complementary kinetic analyses and interfacial or chemical characterization rather than being treated as direct proof of barrier lowering.

This microscopic picture has been further supported at the macroscopic kinetics level and by data-driven modeling. Cai et al.[18] analyzed a large set of MgH_2 dehydrogenation kinetic curves using data-driven methods and reconstructed the conversion-dependent apparent activation energy, $E_a(\alpha)$, by extracting local kinetic parameters via segment-wise fitting. They then representing E_a as a continuous function of conversion, as shown in Figure 2B. Their results show that activation energy is markedly elevated in the early stage of the reaction (approximately the first 10%–20% conversion), then drops rapidly within this limited conversion interval, and subsequently remains at a relatively stable plateau over a broad conversion range (roughly 10%–90%; Figure 2C). This conversion-resolved $E_a(\alpha)$ profile therefore provides an operational kinetic signature of the burst effect. Importantly, some experimental dehydrogenation curves from catalyst- and alloy-modified MgH_2 samples (for example MgH_2-Ni_3C, MgH_2-Nb_2O_5, Mg_2Ni_4, and MgIn) were also examined in this study. Their activation energy profiles display the same initial decline followed by stabilization, further reinforcing the generality of the burst effect across different material systems. Taken together, these observations suggest that the conversion-resolved $E_a(\alpha)$ trend represents a robust kinetic pattern at the materials level rather than an artifact of a single dataset or protocol. Nevertheless, the visibility of this $E_a(\alpha)$ signature can depend on the experimental regime and the length scale. In materials screening and laboratory kinetic measurements, heat transfer effects are often negligible because the sample mass is small and thermal contact is usually well controlled. However, at the scale of reactors or devices, the influence of heat transfer limitations and temperature gradients may be amplified, which can blur kinetic features that vary with reaction progress and thereby obscure the burst effect signature; therefore, observing the burst effect under such conditions requires carefully designed experiments.

In this study, Cai et al. also surveyed a large body of literature and found that dehydrogenation barriers from DFT calculations, which mostly correspond to pristine MgH_2 and surface H desorption, are generally higher, with an average of 214.4 $kJ{\cdot}mol^{-1}$ (~2.22 eV), whereas the apparent activation energies obtained from experimental fitting are generally lower, with an average of 135.9 $kJ{\cdot}mol^{-1}$ (~1.41 eV), as shown in Figure 2A. When these statistics are compared with their fitted $E_a(\alpha)$ profiles, the early-stage $E_a(\alpha)$ values often fall within the range reported by theoretical calculations, while the Ea(α) values in the stable regime (plateau or near-equilibrium regime) converge toward the range obtained from experimental fitting. On this basis, they inferred that the systematic difference between DFT barriers and apparent activation energies from macroscopic kinetic fitting mainly reflects that the two approaches emphasize different stages. DFT calculations are often well suited to resolving the early stage, in which H_2 desorption from the surface hydrogen layer requires overcoming a high barrier. By contrast, macroscopic fitting is frequently dominated by later, lower-barrier stages, so the brief early high-barrier period contributes less to the overall fitted activation energy. Notably, the deviation quantified in this work between DFT-computed barriers and the apparent activation energies derived from macroscopic kinetic fitting aligns well with the layer-by-layer dehydrogenation picture reported by Dong et al.,[17] showing close numerical agreement (Figure 2A). This agreement thus lends additional support to the above interpretation and provides corroborating evidence for the burst effect.

Building on this insight, the authors further proposed a burst-effect-based demand-driven dynamic heating (DDDH) strategy,[21] in which the heat input is temporarily intensified during the early high-barrier stage and reduced after the burst stage. Unlike a generic thermal-management optimization, DDDH is formulated to match heat supply to the stage-dependent kinetic demand, so that the early triggering step is preferentially assisted while unnecessary high-temperature residence is avoided. To enable a fixed-energy comparison, the reported analysis emphasizes metrics, such as the time to reach a fixed release fraction at a prescribed energy budget or equilibrium temperature, rather than performance gains under arbitrarily tailored heating profiles. With respect to scalability, the effectiveness of DDDH can be constrained by heat-transfer limitations and temperature gradients at larger reactor scales, which may blur the stage-specific kinetic demand; practical implementation therefore requires sufficient control bandwidth and sensor signals to track temperature and infer reaction progress for robust switching.

EXPERIMENTAL ADVANCES IN CATALYST-ASSISTED MgH_2 DEHYDROGENATION

Numerous experimental studies have shown that suitable catalysts can substantially lower the dehydrogenation temperature of MgH_2 while maintaining a practically meaningful reversible capacity at the composite level. Here, we summarize representative catalyst systems that have been validated by experiments. Unless otherwise stated, hydrogen capacities discussed here follow the reporting conventions adopted in the original studies and typically correspond to composite-level values. It is important to note that reported MgH_2 dehydrogenation metrics depend strongly on experimental protocol, so direct comparisons of absolute values across different studies are often not meaningful. This limited comparability arises from differences in experimental design and data reporting practices across the literature. Where key experimental metadata are not reported in the original studies, we note this limitation, but we do not use such data for cross-study benchmarking. Reported performance values are therefore discussed to highlight improvements relative to the baseline used within each individual study rather than as a basis for ranking catalyst systems. Generally, equilibrium thermodynamic quantities measured under defined

Please cite this article in press as: Gao et al., Catalytic strategies and mechanisms for enhancing MgH_2 solid-state hydrogen storage, Chem Catalysis (2026), https://doi.org/10.1016/j.checat.2026.101692

conditions tend to be more comparable across laboratories, whereas kinetic metrics such as onset temperature or peak temperature from differential scanning calorimetry (DSC) are often more protocol dependent. To improve reproducibility, we encourage minimum reporting requirements where feasible, including replicate measurements and uncertainty estimates, together with instrument calibration details, particle-size distributions, and cycling history.

In addition, a lower DSC peak temperature at a fixed heating rate reflects combined thermal and kinetic factors and should not be taken as direct evidence of reduced intrinsic activation barriers. Mechanistic interpretations based solely on peak temperature changes should therefore, where possible, be corroborated by complementary kinetic analyses, *in situ* or *operando* evidence, or both.

Transition-metal and transition-metal-oxide catalyst systems

For transition-metal and transition-metal-oxide catalyst systems, a common strategy is to introduce nanometer-scale transition metals and their oxides into MgH_2 to construct highly dispersed, interconnected interfacial catalytic networks, thereby markedly improving its dehydrogenation performance. For example, Zhang et al.[22] introduced 5 wt % amorphous multivalent NbH_x nanoparticles into MgH_2 by ball milling. In the same study, the MgH_2/c-NbH_x composite shows a reduced DSC peak dehydrogenation temperature from 365.5°C to 273.0°C, desorbs 7.0 wt % H_2 within 9 min at 300°C, and exhibits an apparent desorption activation energy of 50.4 ± 0.6 kJ·mol^{-1} H_2. For the nanosheet-like $Co_3V_2O_8$ catalyst prepared by Long et al.,[23] Figure 3A shows that, in the dehydrogenated state, Co and V_2O_3 nanophases are uniformly attached to the Mg/MgH_2 surface, providing continuous interfacial pathways for hydrogen diffusion. The optimal $Co_3V_2O_8$ content in MgH_2 is 6 wt %. Under the corresponding testing conditions, the resulting MgH_2-6CoVO composite releases 5.94 wt % H_2 within 5 min at 300°C and still desorbs 3.41 wt % H_2 within 120 min at 225°C, while its dehydrogenation activation energy is reduced to 68.5 kJ·mol^{-1}. Abdul Rahman et al.[24] ball milled MgH_2 with various Nb-type catalysts and 5 wt % $KNbO_3$. Figure 3B compares the dehydrogenation curves and shows that MgH_2 + 5 wt % $KNbO_3$ desorbs 3.9 wt % H_2 within 10 min, whereas as-milled MgH_2 and MgH_2 + 10 wt % Nb_2O_5 release only 0.66 and 3.2 wt % H_2, respectively, demonstrating a clear improvement in desorption kinetics relative to the corresponding baseline samples. Taken together, these studies consistently indicate that, within their respective experimental frameworks, constructing highly dispersed interfacial catalytic networks based on transition-metal and transition-metal-oxide nanophases is an effective approach to improving the dehydrogenation kinetics of MgH_2 in the medium-temperature range.

Supported and nanostructure-reinforced catalyst systems

Initially, most attempts to improve the dehydrogenation kinetics of MgH_2 relied on directly doping transition metals and/or their oxides into the MgH_2 matrix (typically by ball milling) to lower the dehydrogenation enthalpy and apparent activation energy. Subsequently, research has shifted from simple doping to nano-confined and support-reinforced architectures where MgH_2 is embedded in carbon-, oxide-, or alloy-based scaffolds decorated with transition-metal active sites. For example, Zeng et al.[27] used a cation-exchange resin as the carbon precursor to prepare a carbon-supported Ni_3S_2 composite catalyst (Ni_3S_2@C). In the same study, when 10 wt % Ni_3S_2@C-4 was added to MgH_2, the resulting MgH_2-Ni_3S_2@C-4 composite released 6.15 wt % H_2 within 8 min at 300°C and, after rehydrogenation, could still desorb 6.35 wt % H_2 at 275°C. The apparent activation energy for hydrogenation decreased from 93.6 to 39.6 kJ·mol^{-1} relative to the corresponding MgH_2 baseline reported in that work, highlighting the strong catalytic effect of the carbon-supported multiphase interface. Oxygen-vacancy-rich 2D TiO_2 nanosheets were obtained by a surfactant-assisted solvothermal route and then used as scaffolds to grow *in situ* nano-MgH_2, forming a flower-like MgH_2/TiO_2 heterostructure. Under the testing conditions employed in that study, this nano-confined architecture lowers the onset desorption temperature from 295°C to 180°C, reduces the apparent activation energy to 106.7 kJ·mol^{-1} H_2, boosts the initial desorption rate at 300°C by 35 times, and delivers 98.5% capacity retention after 100 cycles.[11] Li et al.[25] further employed hierarchically structured Co@C-*x* (*x* = S, M, or L) catalysts for MgH_2. As shown in Figure 3C, the non-isothermal dehydrogenation curves of MgH_2-Co@C-*x* shift markedly to lower temperatures, with MgH_2-Co@C-S decomposing at 194°C instead of 370°C while retaining 6.5 wt % H_2. The derivative curves in Figure 3C give peak desorption temperatures of 280°C, 307°C, and 329°C, and the Kissinger analysis in Figure 3D yields activation energies of 91.5, 98.8, and 103.4 kJ·mol^{-1}, confirming a clear particle-size-dependent reduction of the Mg-H dehydrogenation barrier. Taken together, these examples indicate that, from resin-derived carbon to metal-organic framework (MOF)-derived composite supports, different types of porous and nanostructured supports, although distinct in chemical composition and synthetic routes, share common structural features: they all construct highly dispersed, interconnected multiphase interfaces that shorten hydrogen diffusion pathways and optimize heat and mass transport, thereby enabling fast and reversible hydrogen sorption at reduced operating temperatures.

Multicomponent catalyst systems with finely tuned electronic structure

In the field of multicomponent and electronically engineered complex catalyst systems, recent experimental studies have evolved from simple metal oxides to catalysts with multielement, multiphase interfaces. Yuan et al.[28] synthesized Ni@Pt core-shell nanoparticles and incorporated 10 wt % Ni@Pt into MgH_2 by ball milling. High-angle annular dark-field scanning transmission electron microscopy (HAADF-STEM) and selected-area electron diffraction (SAED) revealed fragmented Ni@Pt particles that evolved into Pt and Ni nanoclusters and reaction products Mg_3Pt and Mg_6Ni, forming intimate metal/MgH_2 interfaces. In the same study, with 10 wt % Ni@Pt, the onset dehydrogenation temperature of MgH_2 decreased from 328°C to 210°C, dehydrogenation finished at around 300°C, and the apparent activation energy dropped from 165.1 to 89.9 kJ·mol^{-1}, markedly

Please cite this article in press as: Gao et al., Catalytic strategies and mechanisms for enhancing MgH_2 solid-state hydrogen storage, Chem Catalysis (2026), https://doi.org/10.1016/j.checat.2026.101692

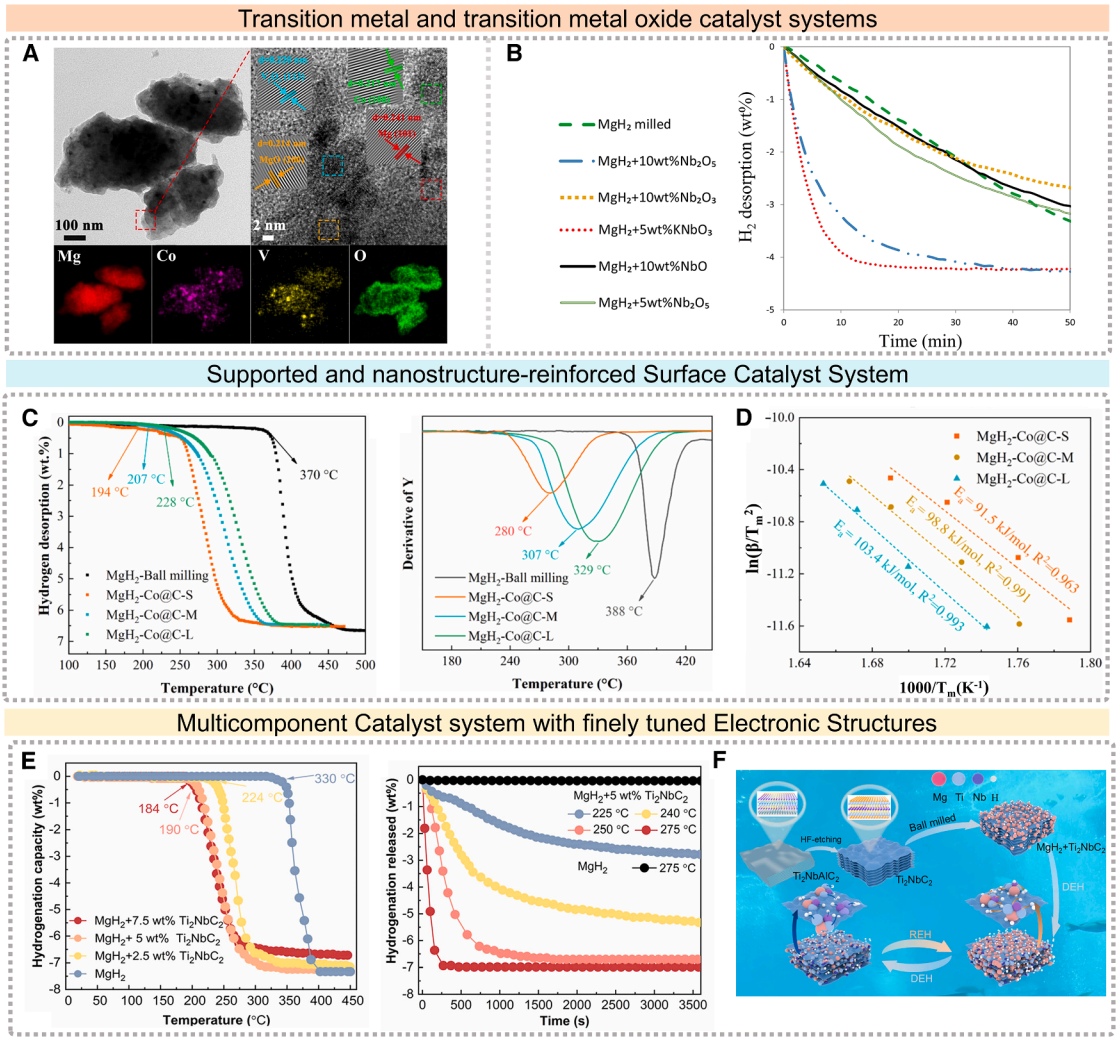

Figure 3. Experimental investigations of catalysts promoting MgH_2 dehydrogenation

(A) High-resolution transmission electron microscopy (HRTEM) and energy-dispersive X-ray spectroscopy (EDS) images of the dehydrogenated state of an MgH_2-6CoVO composite. Reprinted with permission from Long et al.[23] Copyright 2024 Elsevier.

(B) The influence of different Nb-type catalysts on the dehydrogenation of MgH_2. Reprinted with permission from Abdul Rahman et al.[24] Copyright 2019 Elsevier.

(C) Non-isothermal dehydrogenation diagrams of MgH_2-Co@C-*x* (*x* = S, M, or L) and pristine MgH_2.

(D) Kissinger plot of $\ln(\beta/T_m^2)$ versus 1,000/Tm for MgH_2-Co@C-*x* (*x* = S, M, or L). Reprinted with permission from Li et al.[25] Copyright 2025 Elsevier.

(E) Non-isothermal desorption curves of MgH_2 and MgH_2 + *m* wt % Ti_2NbC_2 (*m* = 2.5, 5, or 7.5); isothermal hydrogen desorption curves of pure MgH_2 and MgH_2 + 5 wt % Ti_2NbC_2 at different temperatures.

(F) Mechanism diagram of de-/rehydrogenation of the Ti_2NbC_2-catalyzed MgH_2/Mg system. Reprinted with permission from Lv et al.[26] Copyright 2025 Elsevier.

improving dehydrogenation kinetics and reducing thermal stability.

For the MgH_2-7 wt % $TiNb_2O_7$ composite,[29] under the experimental conditions employed in that study, the onset dehydrogenation temperature decreased from 300°C to 177°C. Approximately 5.5 wt % H_2 was released within 10 min at 250°C, and a reversible hydrogen storage capacity of 4.5 wt % was achieved at 150°C. When Ti and Nb were transferred from an oxide framework to a carbide framework, Lv et al.[26] synthesized Ti_2NbC_2 MXene by etching Ti_2NbAlC_2 in hydrofluoric acid (HF) and introduced 5 wt % Ti_2NbC_2 into MgH_2 by ball milling. In the non-isothermal tests (Figure 3E), MgH_2 + 5 wt % Ti_2NbC_2 exhibited an onset and end dehydrogenation temperatures of 190°C and 275°C instead of 330°C and 400°C for pristine MgH_2 in this study, while still releasing 6.9 wt % H_2. The isothermal curves in Figure 3E further reveal that at 275°C the composite desorbed 6.9 wt % H_2 within 250 s, whereas MgH_2 remained almost inert. The mechanism illustration in Figure 3F links this acceleration to *in situ* TiH_2 and NbH "hydrogen pumps" and conductive Ti_2NbC_2 layers that weaken interfacial Mg-H bonds and create fast H^- diffusion pathways. For an even higher level of compositional complexity, Pan and colleagues[30] introduced a 5 wt % FeCoNiCrMn high-entropy alloy (HEA) into MgH_2, lowering the onset dehydrogenation temperature from 278.2°C to 209.1°C.

Please cite this article in press as: Gao et al., Catalytic strategies and mechanisms for enhancing MgH_2 solid-state hydrogen storage, Chem Catalysis (2026), https://doi.org/10.1016/j.checat.2026.101692

The resulting composite released 5.6 wt % H_2 within 10 min at 280°C and retained 98.6% of its effective capacity after 50 cycles as evaluated relative to the corresponding MgH_2 reference in that study.

Taken together, these multicomponent, electronically tunable catalysts construct multimetal, multivalent nanointerfaces that synergistically optimize hydrogen diffusion and interfacial charge transfer, thereby substantially lowering the dehydrogenation temperature and activation barriers.

THEORETICAL INSIGHTS INTO MECHANISMS UNDERLYING CATALYZED DEHYDROGENATION OF MgH_2

Intrinsic dehydrogenation mechanism of MgH_2

DFT calculations indicate that the intrinsic kinetic bottleneck for dehydrogenation of stoichiometric MgH_2 is mainly associated with surface processes. Du et al.[31] computed H_2 recombinative desorption on low-index MgH_2 surfaces such as (001) and (110) and found that, even on the most favorable (110) facet, the activation barrier is still about 1.8 eV, whereas other pathways are generally above 2.0 eV, indicating that ideal MgH_2 surfaces are inherently difficult to dehydrogenate. Chen et al.[32] further compared the surface energies, hydrogen diffusion barriers, and hydrogen-vacancy formation energies of different facets and showed that realistic MgH_2 particles tend to expose stable low-energy surfaces such as (110), which, however, are the least favorable for forming H vacancies and enabling surface diffusion, thus making the onset of dehydrogenation difficult. Together with the previously discussed burst effect on the dynamically evolving MgH_2 (110) surface,[17] these results point to the need for surface engineering to overcome the intrinsic dehydrogenation bottleneck of MgH_2, for example, by tuning facet exposure, introducing defects and interfaces, or adding surface catalytic phases, thereby effectively lowering surface-related energy barriers.

Catalytic mechanism of MgH_2 dehydrogenation

Recent advances have proposed several representative mechanistic pictures to rationalize how catalysts accelerate MgH_2 dehydrogenation. These pictures do not invoke fundamentally different intrinsic reaction pathways but rather emphasize different aspects of interfacial chemistry and structure highlighted in specific catalyst systems. Some studies have proposed that multicomponent catalysts may function as ''hydrogen pumps,'' providing a conceptual framework to rationalize the accelerated dehydrogenation of MgH_2. As a representative example for rationalizing interfacial effects, in the oxygen-vacancy-rich H-V_2O_5 system,[33] density of states (DOS) calculations in Figure 4A show that introducing oxygen vacancies shifts the d-band center of the MgH_2-V_2O_{5-x} interface toward the Fermi level, increases electron density, and weakens both Mg-H and V-H bonds, thereby lowering the dehydrogenation barrier. The schematic in Figure 4B illustrates a proposed V/VH_2 hydrogen pump cycle, in which reversible hydrogen exchange at vacancy-rich interfaces is suggested to facilitate interfacial H transport and promote MgH_2 decomposition. Similarly, $Mn_{1.48}Ti_{1.1}V_{0.3}Zr_{0.12}$ nanosheets have been proposed to exhibit hydrogen pump behavior, in which hydrogen dissociation at relatively low temperatures and the coupled exchange of hydrogen and electrons are suggested to facilitate interfacial transport. They create intimate MgH_2/MnTiVZr interfaces and fast diffusion paths, suggesting a shift of the RDS from surface penetration to bulk H diffusion and triggering a burst-effect dehydrogenation with reduced kinetic barriers.[19] Together, these studies suggest that electronically tuned, hydrogen pump functionality catalysts provide a plausible mechanistic picture for accelerating MgH_2 dehydrogenation kinetics, although direct *operando* validation of the proposed cycles remains limited.

In Huang and colleagues' works,[34,37] single-atom Ni on TiO_2 ($Ni_{0.034}$@TiO_2) accelerates MgH_2 dehydrogenation by building a Ni-O-Ti^{x+} interface that mediates electron transfer between H^- and Mg^{2+}. X-ray photoelectron spectroscopy (XPS) analysis of MgH_2 in contact with Ni@TiO_2-OV shows that Ni induces multivalent Ti species and abundant oxygen vacancies, while DFT-based COHP and projected DOS (PDOS) analyses indicate that MgH_2 in contact with Ni@TiO_2-OV has the lowest integrated COHP (-ICOHP) and thus the weakest Mg-H bonds among all tested catalysts. Figure 4C depicts a dehydrogenation pathway in which H^- at the MgH_2 surface delivers electrons through the Ni-O-Ti^{x+} centers and vacancy network; Mg-H bonds at the interface are activated and cleaved, interfacial H atoms recombine to H_2, and Mg atoms nucleate. Overall, single-atom Ni activates Mg-H, while Ti^{x+} and vacancies shuttle electrons at the interface during dehydrogenation. In $Ru_{0.028}$@Nb_2O_5, an analogous single-atom-oxide interface controls MgH_2 dehydrogenation. $Ru^{\delta+}$ substitution promotes $Nb^{5+}/Nb^{4+} \rightarrow Nb^{2+}/Nb^0$ redox and abundant oxygen vacancies, building an electron-conductive substoichiometric niobium oxide (NbO_x) matrix. DFT-based COHP/PDOS calculations show that MgH_2 at the Ru@Nb_2O_5-OV interface has markedly reduced Mg-H bond energy and weakened H/Mg orbital overlap, while DOS and impedance analyses confirm an upshifted d-band center and much lower charge-transfer resistance. Consequently, Ru single atoms weaken interfacial Mg-H bonds and accelerate electron flow from H^- to Mg^{2+}, thereby lowering the activation barrier for H_2 desorption.

In the PdNi metallene-derived catalyst,[35] DFT calculations identify PdNi alloy clusters as the most efficient MgH_2 dehydrogenation sites. Figure 4D correlates the d-band centers of surface species with H-vacancy formation energies: PdNi clusters show the most downshifted d-band center and the lowest, even negative, H-vacancy energies, whereas Pd or Ni single atoms and monometallic clusters remain much less active. This d-band shift weakens Mg-H bonding and destabilizes interfacial hydrides, enabling easier H escape and a lower kinetic barrier for H_2 desorption. This mechanism differs from the previous ones in that it directly engineers H-vacancy formation and H adsorption/desorption strength through d-band center tuning of bimetallic clusters.

Overall, the catalytic strategies discussed above can be viewed as three recurrent mechanistic motifs that describe how interfacial structures are leveraged to promote MgH_2 dehydrogenation: (1) hydrogen pump phases (e.g., Mg_2Ni) integrated with conductive scaffolds to form cooperative H^-/e^- transport

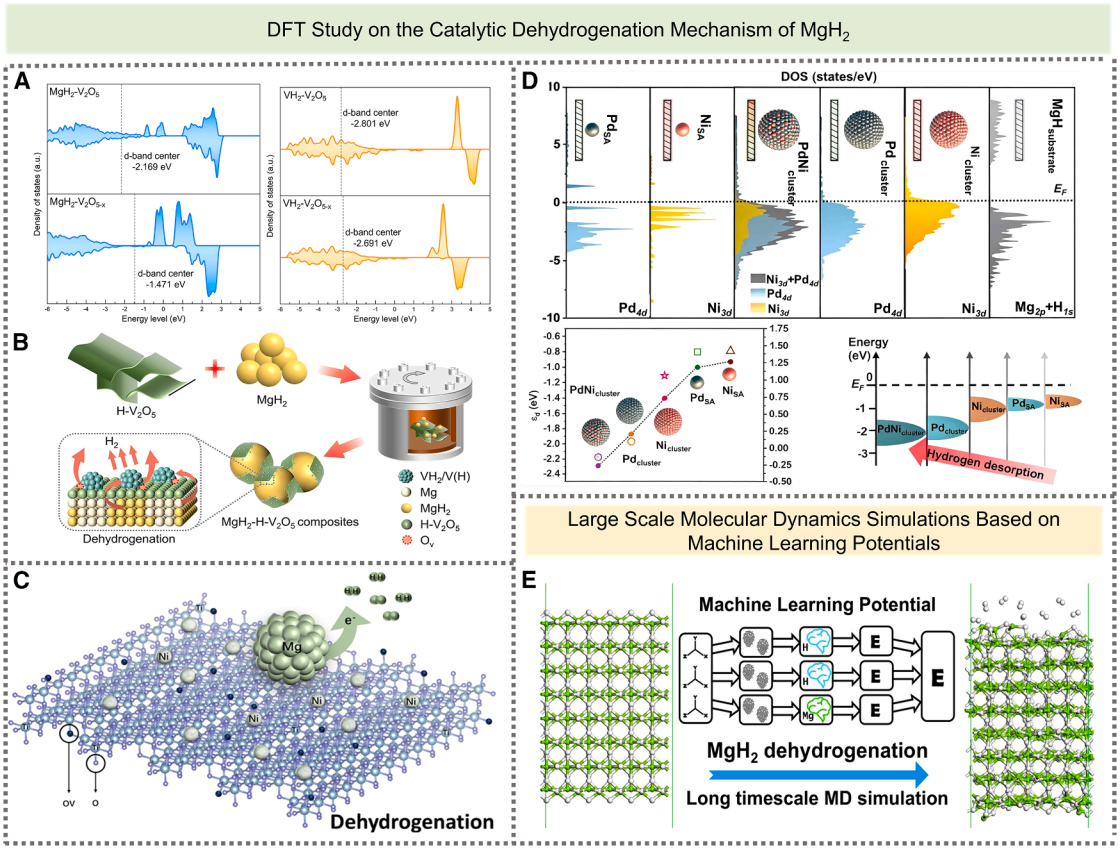

Figure 4. The atomistic mechanism underlying catalyzed dehydrogenation of MgH_2

(A) DOS of the MgH_2-V_2O_5/V_2O_{5-x} system and the VH_2-V2O5/V_2O_{5-x} system.

(B) Schematic diagram showing the mechanisms of enhanced hydrogen storage performance of the MgH_2-H-V_2O_5 composites. Reprinted with permission from Ren et al.[33] Copyright 2024 Springer.

(C) Proposed dehydrogenation mechanism of MgH_2 catalyzed by single-atom Ni supported on oxygen-vacancy-rich TiO_2 (Ni@TiO_2-OV). Reprinted with permission from Zhang et al.[34] Copyright 2024 American Chemical Society.

(D) Electronic structure analysis of the MgH_2 system, including the d-projected density of states (d-PDOS) of Mg 2p and different active sites (SA, single atom), the correlation between d-band center position and hydrogen atom formation energy, and the correlation between d-band center position and the Fermi level during hydrogen desorption. Reprinted with permission from Xu et al.[35] Copyright 2023 Wiley-VCH.

(E) Schematic of machine learning potentials enabling long-timescale MD simulations of MgH_2 dehydrogenation. Reprinted with permission from Morrison et al.[36] Copyright 2024 American Chemical Society.

networks; (2) interfaces formed by oxide-supported single-atom sites with oxygen vacancies and multivalent cations that facilitate interfacial electron redistribution and vacancy-mediated charge transfer, thereby promoting Mg-H bond activation at the interface; and (3) d-band engineered bimetallic clusters focused on tuning the intrinsic hydrogen binding and vacancy formation properties at metal MgH_2 interfaces. These motifs provide a useful conceptual organization of current experimental and theoretical studies. In practical catalyst systems, multiple motifs often coexist, and their relative importance may evolve with temperature, microstructure, and operating conditions. Across these motifs, a unifying perspective is that many of the proposed surface and interfacial interventions can also be discussed within the burst-effect framework, in which improved dehydrogenation kinetics may be interpreted as reducing the effective barrier associated with the surface dehydrogenation step.

Investigating the dehydrogenation mechanism by large-scale molecular dynamics simulations based on machine learning potentials

While DFT has played a central role in revealing dehydrogenation mechanisms of MgH_2, its predictions typically depend on specific modeling choices, including surface termination, defect density, slab thickness, and the treatment of temperature. In practice, DFT is therefore more reliable for comparing relative trends under consistent assumptions rather than for quantitatively predicting absolute dehydrogenation temperatures. These inherent limitations indicate the need for complementary approaches that can operate at larger length and time scales and under finite temperature conditions. Among these, the use of interatomic potentials trained with machine learning in large-scale molecular dynamics (MD) simulations has become an increasingly adopted approach.

In recent years, machine learning interatomic potentials (MLIPs) combined with large-scale MD simulations have been

Please cite this article in press as: Gao et al., Catalytic strategies and mechanisms for enhancing MgH_2 solid-state hydrogen storage, Chem Catalysis (2026), https://doi.org/10.1016/j.checat.2026.101692

increasingly used to investigate hydrogen diffusion and phase transformations in Mg/MgH_2 systems.[38] For example, Angeletti et al.[39] constructed an Mg-H database using an active-learning workflow based on a Vienna Ab initio Simulation Package (VASP)-based machine learning force field (VASP-MLFF) and compared several MLIPs, including VASP-MLFF, Message Passing Atomic Cluster Expansion (MACE), and the Crystal Hamiltonian Graph Neural Network (CHGNet). Their strategy yields diffusion coefficients and activation energies that are in good agreement with experiments over a wide range of hydrogen contents and temperatures, suggesting that carefully constructed and iteratively refined MLIPs can reasonably capture the diffusion kinetics of Mg-H systems.

By contrast, studies that explicitly employ MLIPs in combination with large-scale MD to simulate the full dehydrogenation process of MgH_2 are still relatively scarce. A particularly illustrative example is the work of Morrison et al.,[36] who developed a Behler-Parrinello-type charge-equilibrated neural network potential (C-NNP) MLIP (Figure 4E) trained on a large database covering diverse Mg/MgH_2 structures and used it to perform nanosecond-scale MD simulations on a thick $MgH_2(110)$ slab. The model exhibits satisfactory generalization and enables long-timescale dynamical simulations. The long MD trajectories obtained with this potential reveal that H_2 molecules tend to form as subsurface species and remain trapped there for extended periods. On this basis, the authors proposed that such ''subsurface H_2 formation and trapping'' may be an important origin of the sluggish dehydrogenation kinetics of MgH_2.

Overall, combining high-accuracy MLIPs with large-scale MD simulations may make it possible to approach near-first-principles accuracy while substantially extending the accessible spatial and temporal scales, thereby providing a more explicit finite-temperature description of hydrogen behavior in MgH_2. At the current stage, such simulations are relatively reliable for directly tracking finite-temperature phenomena that occur within the accessible time window, such as surface or interfacial reconstruction, diffusion events, and early nucleation-related structural changes. However, quantitatively resolving rare-event kinetics or extracting accurate barriers and absolute rates without enhanced sampling remains challenging and should be interpreted with caution. Nevertheless, when used with appropriate safeguards and experimental cross-checks, MLIP-enabled long-timescale MD remains a valuable complementary approach for mechanistic studies beyond conventional DFT.

THEORY-GUIDED DESIGN FOR MG-BASED HYDROGEN STORAGE MATERIALS AND CATALYSTS

Building on the mechanistic insights developed in the previous sections, which range from the burst effect at MgH_2 surfaces to atomistic pictures obtained from DFT calculations, it is natural to ask how theory can be used not only to rationalize existing experiments but also to guide the design of improved magnesium-based hydrogen storage materials and their catalysts. In this section, we discuss two complementary, theory-driven routes: (1) direct design of Mg-based hydrides and catalytic interfaces using first-principles calculations and (2) descriptor-based strategies that translate calculated properties into practical design rules and, where appropriate, into data-driven screening protocols.

Direct theory-driven design of MgH_2 materials and catalysts

Direct theory-driven design focuses on using first-principles calculations not only to interpret experimental observations but also to propose concrete architectures for MgH_2 materials and catalysts in advance. Li et al.[40] employed DFT calculations to determine the energy barriers for H_2 diffusion and H-H recombination, as well as the Nb/H charge distribution, in MgH_2/NbO_x systems with different Nb oxidation states. As shown in Figure 5A, slightly oxidized Nb forms a stable local H-Nb state on the surface and simultaneously minimizes the barriers of both steps. On this basis, the authors proposed that Nb_2O_5 should be partially reduced to NbO_x phases with oxidation states close to Nb_2O_3, which act as preferred active species for catalyzing MgH_2 dehydrogenation.

Within the broader concept of carbon-based confinement, Zhang et al.[43] used DFT to investigate MgH_2 clusters supported on pristine graphene and on defect- or heteroatom-modified graphene. They computed the formation enthalpies of the modified graphene, the dehydrogenation enthalpy of MgH_2, the cluster-graphene binding energies, and the dehydrogenation activation energies and combined these with charge analysis to evaluate how doping perturbs the Mg-H bonds. The results indicate that B- and P-doped graphene can markedly lower both the thermodynamic and the kinetic barriers of dehydrogenation while strengthening the confinement effect; among these, B doping is the most effective and was therefore suggested as a preferred support for MgH_2 nanoparticles. Building on the ''impurity junction'' concept, Li et al.[41] further constructed MgH_2/graphene and B-doped, P-doped, and B/P-codoped graphene impurity junctions. They calculated the reaction energies and energy barriers for the release of a single H_2 molecule and performed Mulliken charge analysis of charge transfer from MgH_2 to the carbon framework. For the MgH_2/BPG system (MgH_2 supported on B/P-codoped graphene), dehydrogenation proceeds via a P-H intermediate in two steps, with a maximum barrier of only about 0.7 eV, which is significantly lower than that of the undoped interface (Figure 5B). This demonstrates that B/P-codoped graphene can simultaneously weaken Mg-H bonds and provide stable H intermediate sites and was thus proposed as a priority support design for MgH_2/carbon composite hydrogen storage materials.

By further integrating single-atom catalysis with carbon-based confinement, using DFT calculations, Yang and colleagues[44] designed MgH_2/γ-graphyne single-atom catalyst (SAC) systems (GY-SAC-TM, TM = V, Cr, Mn, Fe, Co, Ni, Cu, or Zn) and evaluated their dehydrogenation free-energy profiles and activation barriers as key design metrics. The dehydrogenation barrier of pristine MgH_2 (~2.5 eV) is markedly reduced on GY-SAC-TM; among the screened transition metals, the Fe single-atom system shows the lowest barrier (~0.7 eV) and therefore is identified as the most promising catalytic center. Duan et al.[42] examined TM SA-N-carbon nanotubes (CNTs)-$MgH_2(110)$ interfaces and used nudged elastic band (NEB) calculations to obtain the dehydrogenation barriers of first-layer bridging H atoms adjacent to the single-atom

Please cite this article in press as: Gao et al., Catalytic strategies and mechanisms for enhancing MgH_2 solid-state hydrogen storage, Chem Catalysis (2026), https://doi.org/10.1016/j.checat.2026.101692

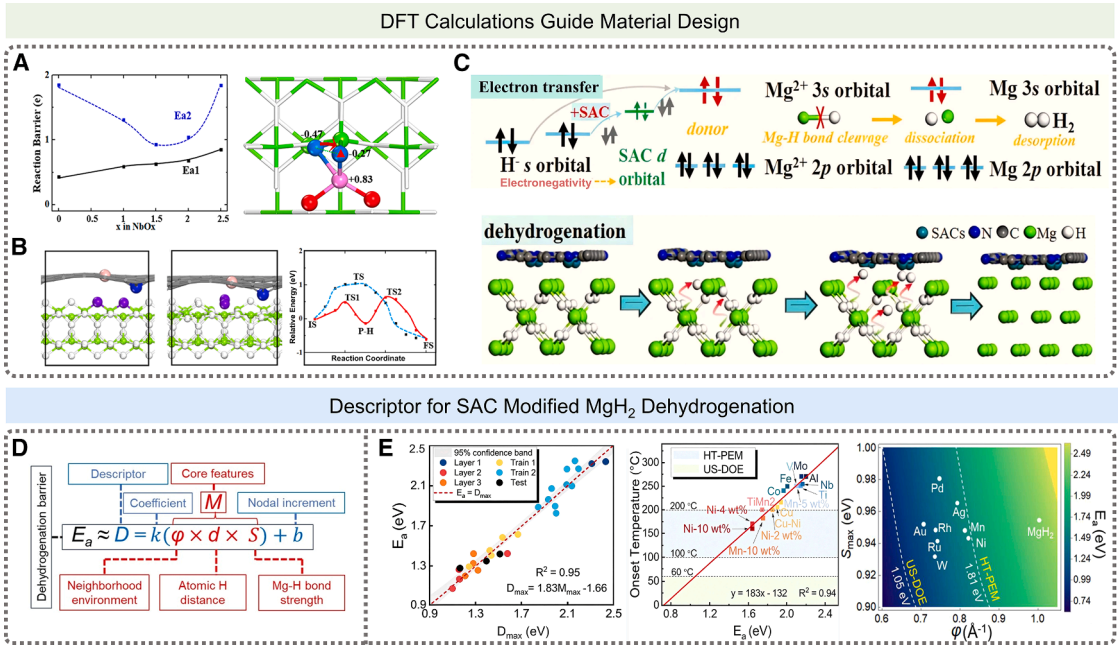

Figure 5. Theory-guided design strategies for materials and catalysts

(A) DFT-based mechanistic understanding of NbO_x-modified MgH_2. Reprinted with permission from Li et al.[40] Copyright 2021 American Chemical Society.

(B) Hydrogen release from the MgH_2/BPG heterojunction. From left to right are the initial configuration, the final configuration after H_2 desorption, and the corresponding reaction energy profile. Reprinted with permission from Li et al.[41] Copyright 2021 American Chemical Society.

(C) The dehydrogenation mechanism of the TM SA-N-CNTs-MgH_2, where CNTs denotes carbon nanotubes. Reprinted with permission from Duan et al.[42] Copyright 2025 Elsevier.

(D) Descriptors that may affect the MgH_2 dehydrogenation kinetics, where E_a represents the dehydrogenation energy barrier of MgH_2 and D represents the descriptor of energy barrier. φ, d, and S represent the parameters composed of the neighboring environment, H-H distance, and Mg-H bonding strength, respectively. M represents the part of the model that contains basic parameters (i.e., φ, d, and S). k and b are the coefficients and intercepts that linearly connect with M and D, respectively.

(E) Validation and application of a data-driven descriptor for MgH_2 dehydrogenation. The left shows the correlation between the calculated activation energy (E_a) and the descriptor D_{max}. The middle gives the correlation between onset dehydrogenation temperature and dehydrogenation barrier, and the derived contour plot predicts the dehydrogenation energy barrier of metal-doped MgH_2 as a function of S_{max} and φ. Reprinted with permission from Li et al.[20] Copyright 2024 Wiley-VCH.

sites. The results reveal that the introduction of TM SA-N-CNTs can substantially lower the MgH_2 dehydrogenation barriers, with the Cr-based system giving the lowest value of 1.18 eV. Based on H-site DOS, electron localization function (ELF), differential charge density, and orbital-resolved analyses, the authors argued that the TM d orbitals on the N-doped CNT backbone construct an efficient electronic coupling pathway, enabling electrons of surface hydride species to be transferred stepwise via the single atom and the carbon scaffold to Mg^{2+}. This process weakens the Mg-H bonds and promotes dehydrogenation. Figure 5C schematically illustrates this "electron cableway" mechanism, on the basis of which Cr SACs anchored on N-doped CNT confinement frameworks were recommended as priority designs for improving the dehydrogenation kinetics of MgH_2.

DFT also becomes a powerful screening tool for analyzing MgH_2 destabilization. Kuganathan et al.[45] systematically calculated alloy formation energies and dehydrogenation enthalpies for Mg-A systems, pinpointing additives such as Ag, Ge, Sn, and Ni that can thermodynamically lower desorption enthalpy and guide the rational design of Mg-based hydrogen storage alloys. Their work exemplifies how first-principles thermodynamics can narrow the compositional space before costly experimental exploration.

Descriptor-based and data-driven inverse design

Once sufficient mechanistic and performance data accumulate, it becomes possible to replace repeated full DFT workflows with low-dimensional descriptors and data-driven surrogates that support inverse design. Fu et al.[46] combined DFT calculations with electronic-structure analysis to identify the ionicity index, defined as the Bader charge transferred per valence electron, as an effective descriptor for metal hydride dehydrogenation. They reported a clear threshold: when the ionicity index falls below 0.77, γ-MgH_2 undergoes spontaneous dehydrogenation at 373 K (100°C), outperforming the α-MgH_2 phase.

Building on the notion that descriptors can be system specific, Dong et al.[47] developed a descriptor for MgH_2/SAC heterojunctions based on system electronegativity, an integrated measure of the electronegativities of metal, C, and N atoms and d-orbital electron characteristics. This descriptor correlates linearly with DFT-derived dehydrogenation barriers and captures how lower SAC electronegativity, such as in Ti-based SACs, weakens H-Mg bond polarity and lowers dehydrogenation barriers by up to 2.22 eV. The study also reported a predicted dehydrogenation temperature of 247.65 K for MgH_2/SAC-Ti, estimated from the calculated barriers using the

Please cite this article in press as: Gao et al., Catalytic strategies and mechanisms for enhancing MgH_2 solid-state hydrogen storage, Chem Catalysis (2026), https://doi.org/10.1016/j.checat.2026.101692

Arrhenius equation under a rate-equivalence assumption (with MgH_2 taken as 700 K). To extend this concept beyond single-parameter descriptions, Li et al.[20] introduced a unified descriptor that aggregates Mg-H bond strength (ICOHP), normalized H-H distances, and neighborhood modifications caused by vacancies and dopants, as illustrated in Figure 5D. The model predicts dehydrogenation barriers with high accuracy (R^2 = 0.95, errors $\leq$0.2 eV) and aligns with experimental dehydrogenation temperatures (R^2 = 0.94), as shown in Figure 5E. Besides, white-box AI may further enable the discovery of compact physical or semi-physical equations from data as already demonstrated for metal hydrides in predicting gravimetric hydrogen density and equilibrium pressure.[48] Together, these advances demonstrate how this multivariate formulation supports inverse design by forecasting how dopants such as Mn or Ni shift descriptors toward the United States Department of Energy (US-DOE) target barrier.

Beyond DFT-derived descriptors, data-driven workflows now integrate automated literature mining. Zhang et al.[49] developed a descriptive interpretation of visual expression (DIVE) multiagent workflow, which systematically reads and sorts out experimental data from graphical elements in the literature. They found that the DIVE workflow markedly improves the accuracy and coverage of data extraction (from experimental hydrogen storage materials literature) compared with the direct extraction by multimodal models, with gains of 10%–15% over commercial models and over 30% relative to open-source models. Building on a curated database of >30,000 entries from about 4,000 articles, they established a rapid inverse design workflow that is able to rapidly identify previously unreported hydrogen storage compositions. Yao et al.[50] developed a large language model (LLM) pipeline that extracted catalytic information from 759 publications to build a database of 809 catalysts. Regression models trained on this dataset achieved $R^2 > 0.91$ for predicting dehydrogenation temperatures and activation energies, and a genetic algorithm proposed candidate catalyst compositions consistent with recent experiments. This framework illustrates how descriptor concepts can be scaled through automated data curation and machine learning.

Collectively, these studies demonstrate a clear evolution from single-parameter electronic descriptors to multivariate and system-specific formulations that link atomistic mechanisms with experimental behavior. Such descriptors enable rapid screening of dopants, catalysts, and nanoconfinement architectures and provide the foundation for data-driven inverse design pipelines. As descriptor robustness and data availability continue to improve, integrated DFT-descriptor-machine learning workflows are poised to play an increasingly central role in the rational design of Mg-based hydrogen storage materials.

OUTLOOK

This perspective is organized around the burst effect in MgH_2 dehydrogenation and underscores the rate-limiting nature of the initial surface dehydrogenation step. We have discussed how catalytic strategies reshape this step and, in turn, the overall hydrogen-release kinetics. Despite substantial progress in lowering the dehydrogenation temperature and apparent activation energy of MgH_2, a clear pathway toward practical devices and generally applicable design rules is still lacking. With this in mind, we outline several directions that could help bridge this gap.

Lightweight design under catalyst-loading constraints

For vehicular and other mobile applications, catalyst loading and gravimetric hydrogen capacity are tightly coupled, and this trade-off will remain a central design constraint. This coupling reflects an inherent dilution penalty: increasing additive fraction tends to reduce deliverable gravimetric capacity and therefore imposes a practical upper bound on catalyst loading when system-level targets are considered. Simply increasing catalyst loading to reduce the dehydrogenation temperature is therefore unlikely to be a viable long-term strategy. A more sustainable approach is to develop catalytic systems with intrinsically high activity that can lower the barrier for the first surface dehydrogenation step at very low loadings, for example, by exploiting single-atom sites or ultrathin nanosheets.[51] From a broader energy efficiency perspective, recent coordination-driven studies have emphasized that reducing the energetic cost of catalytic processes depends not on maximizing activity per se but on achieving targeted activation with minimal material and energy input. In this context, catalysts that selectively accelerate the rate-limiting surface step of MgH_2 dehydrogenation are particularly attractive, as they may enable faster hydrogen release without proportionally increasing catalyst loading and may help reduce the practical energy demand associated with initiating hydrogen release.[52] It would also be valuable if future studies reported normalized efficacy metrics, for example, the reduction in dehydrogenation temperature or a characteristic release time per weight percent catalyst loading under a specified protocol, enabling more quantitative comparison across systems.

Joint optimization of catalytic activity and nanoconfinement

Strong nanoconfinement and engineered heterostructures can improve interfacial contact and surface activation, yet excessive confinement can lengthen hydrogen diffusion paths and increase diffusion resistance.[43] This suggests the existence of an "optimal window" linking catalytic strength and the degree of confinement. Systematic tuning of pore size, interfacial adhesion, and particle size, together with *in situ* measurements and multiscale modeling, should allow this optimal window to be mapped in a more quantitative manner. This mapping would, in turn, enable interfacial and structural codesign guided by surface-controlled kinetics. At the same time, increasing catalytic complexity and architectural sophistication inevitably raise questions beyond kinetic performance alone. From a life-cycle perspective, gains achieved through elaborate synthesis routes, multicomponent catalysts, or heavily engineered supports may carry non-negligible environmental costs, highlighting the importance of evaluating storage materials within a full "cradle-to-grave" framework to ensure that improvements in dehydrogenation kinetics translate into net sustainability benefits rather than localized performance gains. Importantly, cost and critical material constraints should be weighed alongside kinetics when "earth-abundant" pathways are emphasized. Accordingly,

catalysts based on abundant elements and manufacturable architectures are more amenable to scale-up, whereas noble metal systems such as Ru or clusters containing Pd should be regarded as proof of principle unless low loadings and recyclability are convincingly demonstrated.[53]

Working-state stability and *in situ/operando* mechanistic insights

Under realistic operating conditions, MgH_2 typically releases hydrogen at 300°C–350°C or above, where the phase state, valence state, and microstructure of catalysts evolve continuously during cycling. In this regime, *ex situ* "before/after" characterization alone is not sufficient to identify the true active structure or the dominant deactivation channels. There is a clear need for *in situ/operando* X-ray diffraction (XRD), X-ray absorption fine structure measurements, electron microscopy, and spectroscopic tools tailored to MgH_2, so that surface activation, interfacial reconstruction, and hydrogen transport can be tracked under working conditions. In parallel, catalysts and supports should be designed with improved thermodynamic and structural stability at high temperature to suppress sintering, phase separation, and irreversible oxidation over repeated cycles.

MLIPs and long-timescale MD simulations

Conventional DFT and classical MD each face a trade-off between accuracy, accessible time/length scales, and computational cost, which limits our ability to follow the full dehydrogenation pathway of MgH_2, especially the evolution of crucial surface events. MLIPs trained on high-quality DFT data provide a route to perform nanosecond-to-microsecond MD simulations at near-first-principles accuracy. Such simulations can monitor the onset of dehydrogenation, interfacial restructuring, and hydrogen diffusion in a continuous fashion and can be cross-checked against *in situ* experiments. Although such quantitative *in situ/operando* benchmarks are not yet routine in the MgH_2 hydrogen storage literature, they represent a valuable next step for turning MLIP-enabled MD from a qualitative microscope into a quantitatively validated predictive tool. Together, they offer a rich data foundation for extracting physically meaningful descriptors and informing subsequent materials design.[36]

Data science with standardized data and robust validation

To enable inverse design guided by mechanism, machine learning must be integrated with high-quality experimental and computational datasets that explicitly link composition, structure, performance, and mechanism. Such integration can reveal descriptors associated with the initial surface dehydrogenation step and support inverse design strategies for identifying new catalysts and interfacial architectures under practical performance constraints.

Progress in this direction depends critically on data quality and comparability, motivating the need for more harmonized testing protocols and shared data standards across the MgH_2 community. Recent community-oriented efforts illustrate how this can be achieved; for example, the large-scale experimental database (namely, the Digital Hydrogen Platform, *DigHyd*: www.dighyd.org) integrated multiagent systems based on the DIVE workflow[49] can rapidly design and validate new metal hydride systems with high performance; the open-access Digital Hydrogen-S platform[54] (http://digital-hydrogen.com/storage/) provides a standardized literature-curated data infrastructure for comparative analysis and data-driven discovery in solid-state hydrogen storage; and the Cat-MH/XPEAK (http://cat-mh.top) framework demonstrates how literature-derived MgH_2 datasets and standardized XRD structural fingerprints can be translated into reproducible machine learning workflows for catalyst screening and performance analysis.[55]

At the same time, descriptor-based and data-driven approaches require careful methodological safeguards. Descriptor validation should extend beyond random training-test splits to assess generalization across catalyst classes or chemistry families together with uncertainty quantification and domain applicability checks. Particular attention should also be paid to the risk of descriptor leakage, where correlated experimental factors such as particle size or synthesis route can spuriously inflate predictive performance.[38,52]

A transferable framework for solid-state hydrogen storage beyond MgH_2

A conceptual view based on the burst effect may be transferable, as a tentative hypothesis, to other solid-state hydrogen storage systems beyond MgH_2. Complex hydrides such as $LiBH_4$ and $NaAlH_4$ often exhibit pronounced kinetic bottlenecks, and their dehydrogenation typically proceeds through multiple steps with evolving local bonding and coordination environments, which may give rise to stage-dependent kinetics.[56] In this context, there may also exist, in some systems, an early surface or interfacial "induction" step that is disproportionately demanding at the beginning, after which subsequent steps may become less constrained once the initial local environment is perturbed. For example, MD simulations based on an MLIP suggest that hydrogenation of CaH_2 may also involve a similar early interfacial induction step.[57] Importantly, any such transferability should be established on the basis of supporting evidence, for example, by identifying the corresponding early-stage bottleneck and demonstrating that descriptors linked to this step remain predictive across materials and catalytic modifications.

ACKNOWLEDGMENTS

This work was supported by the Beijing Natural Science Foundation (2262076), Hebei Natural Science Foundation (E2025502039), and Fundamental Research Fund for the Central Universities (2025JC008 and 2025MS131).

AUTHOR CONTRIBUTIONS

Z.G.: writing – original draft, conceptualization, methodology, and formal analysis. X.Y.: writing – original draft and conceptualization. Z.Z.: writing – original draft, visualization, and methodology. Y.Z.: writing – original draft and visualization. J.C.: writing – original draft and visualization. Y.L.: writing – original draft and formal analysis. W.F.: writing – original draft and formal analysis. H.L.: writing – review & editing and supervision.

W.Y.: writing – review & editing, supervision, project administration, and funding acquisition.

DECLARATION OF INTERESTS

The authors declare no competing interests.

DECLARATION OF GENERATIVE AI AND AI-ASSISTED TECHNOLOGIES IN THE WRITING PROCESS

During the preparation of this work, the authors used ChatGPT in order to polish the grammar. After using this tool, the authors reviewed and edited the content as needed and take full responsibility for the content of the publication.

REFERENCES

1. Hren, R., Vujanović, A., Van Fan, Y., Klemeš, J.J., Krajnc, D., and Čuček, L. (2023). Hydrogen production, storage and transport for renewable energy and chemicals: An environmental footprint assessment. Renew. Sustain. Energy Rev. *173*, 113113.
2. Hossain Bhuiyan, M.M., and Siddique, Z. (2025). Hydrogen as an alternative fuel: A comprehensive review of challenges and opportunities in production, storage, and transportation. Int. J. Hydrogen Energy *102*, 1026–1044.
3. Wang, Y., Xue, Y., and Züttel, A. (2024). Nanoscale engineering of solid-state materials for boosting hydrogen storage. Chem. Soc. Rev. *53*, 972–1003.
4. McQueen, S., Stanford, J., Satyapal, S., Miller, E., Stetson, N., Papageorgopoulos, D., Rustagi, N., Arjona, V., Adams, J., Randolph, K., et al. (2020). Department of Energy Hydrogen Program Plan (No. DOE/EE-2128) (US Department of Energy (USDOE)).
5. Usman, M.R. (2022). Hydrogen storage methods: Review and current status. Renew. Sustain. Energy Rev. *167*, 112743.
6. Klopčič, N., Grimmer, I., Winkler, F., Sartory, M., and Trattner, A. (2023). A review on metal hydride materials for hydrogen storage. J. Energy Storage *72*, 108456.
7. Zhang, X., Lou, Z., Gao, M., Pan, H., and Liu, Y. (2024). Metal hydrides for advanced hydrogen/lithium storage and ionic conduction applications. Acc. Mater. Res. *5*, 371–384.
8. Yartys, V.A., Lototskyy, M.V., Akiba, E., Albert, R., Antonov, V.E., Ares, J.R., Baricco, M., Bourgeois, N., Buckley, C.E., Bellosta von Colbe, J.M., et al. (2019). Magnesium based materials for hydrogen based energy storage: Past, present and future. Int. J. Hydrogen Energy *44*, 7809–7859.
9. Zhang, T., Isobe, S., Wang, Y., Oka, H., Hashimoto, N., and Ohnuki, S. (2014). A metal-oxide catalyst enhanced the desorption properties in complex metal hydrides. J. Mater. Chem. A *2*, 4361–4365.
10. Jain, A., Agarwal, S., Kumar, S., Yamaguchi, S., Miyaoka, H., Kojima, Y., and Ichikawa, T. (2017). How does TiF_4 affect the decomposition of MgH_2 and its complex variants? - An XPS investigation. J. Mater. Chem. A *5*, 15543–15551.
11. Ren, L., Zhu, W., Li, Y., Lin, X., Xu, H., Sun, F., Lu, C., and Zou, J. (2022). Oxygen Vacancy–Rich 2D TiO_2 Nanosheets: A Bridge Toward High Stability and Rapid Hydrogen Storage Kinetics of Nano-Confined MgH_2. Nano-Micro Lett. *14*, 144.
12. Wang, Z., Tian, Z., Yao, P., Zhao, H., Xia, C., and Yang, T. (2022). Improved hydrogen storage kinetic properties of magnesium-based materials by adding Ni_2P. Renew. Energy *189*, 559–569.
13. Yang, Y., Zhang, X., Zhang, L., Zhang, W., Liu, H., Huang, Z., Yang, L., Gu, C., Sun, W., Gao, M., et al. (2023). Recent advances in catalyst-modified Mg-based hydrogen storage materials. J. Mater. Sci. Technol. *163*, 182–211.
14. Ding, Z., Li, Y., Yang, H., Lu, Y., Tan, J., Li, J., Li, Q., Chen, Y., Shaw, L.L., and Pan, F. (2022). Tailoring MgH_2 for hydrogen storage through nanoengineering and catalysis. J. Magnes. Alloy. *10*, 2946–2967.
15. Duan, C., Tian, Y., Wang, X., Wu, J., Liu, B., Fu, D., Zhang, Y., Lv, W., Hu, L., Wang, F., et al. (2023). Anchoring Mo single atoms on N-CNTs synchronizes hydrogenation/dehydrogenation property of Mg/MgH_2. Nano Energy *113*, 108536.
16. Jiang, H., Ding, Z., Li, Y., Lin, G., Li, S., Du, W., Chen, Y., Shaw, L.L., and Pan, F. (2025). Hierarchical interface engineering for advanced magnesium-based hydrogen storage: Synergistic effects of structural design and compositional modification. Chem. Sci. *16*, 7610–7636.
17. Dong, S., Li, C., Wang, J., Liu, H., Ding, Z., Gao, Z., Yang, W., Lv, W., Wei, L., Wu, Y., and Li, H. (2022). The "burst effect" of hydrogen desorption in MgH_2 dehydrogenation. J. Mater. Chem. A *10*, 22363–22372.
18. Cai, J., Wang, H., Tang, X., Miao, Z., Yao, T., Liu, Y., Wang, H., Gao, Z., and Yang, W. (2025). Data-driven evidence for the burst effect in MgH_2 dehydrogenation via analysis of experimental kinetic curves. J. Energy Storage *136*, 118450.
19. Zhang, L., Zhang, J., Zhong, T., Wu, Y., Chen, D., Zhang, T., and Peng, S. (2025). $Mn_{1.48}Ti_{1.1}V_{0.3}Zr_{0.12}$ nano-pumps enhanced burst effect on solid-state hydrogen storage in MgH_2. Int. J. Hydrogen Energy *190*, 152225.
20. Li, C., Yang, W., Liu, H., Liu, X., Xing, X., Gao, Z., Dong, S., and Li, H. (2024). Picturing the Gap Between the Performance and US-DOE's Hydrogen Storage Target: A Data-Driven Model for MgH_2 Dehydrogenation. Angew. Chem. Int. Ed. *63*, e202320151.
21. Cai, J., Jiang, Y., Yao, T., Tang, X., Liu, Y., Xu, Z., Zhao, X., Zhang, B., Gao, Z., and Yang, W. (2025). A demand-driven dynamic heating strategy for ultrafast and energy-efficient MgH_2 dehydrogenation utilizing the "burst effect". J. Energy Storage *130*, 117495.
22. Zhang, L., Xia, X., Xu, C., Zheng, J., Fan, X., Shao, J., Li, S., Ge, H., Wang, Q., and Chen, L. (2015). Remarkably improved hydrogen storage performance of MgH_2 catalyzed by multivalence NbH_x nanoparticles. J. Phys. Chem. C *119*, 8554–8562.
23. Long, S., Qin, Y., Fu, H., Hu, J., Xue, H., Chen, Y., and Pan, F. (2024). Hydrogen storage properties of MgH_2 modified by efficient $Co_3V_2O_8$ catalyst. Sep. Purif. Technol. *341*, 126901.
24. Abdul Rahman, M.H., Shamsudin, M.A., Klimkowicz, A., Uematsu, S., and Takasaki, A. (2019). Effects of $KNbO_3$ catalyst on hydrogen sorption kinetics of MgH_2. Int. J. Hydrogen Energy *44*, 29196–29202.
25. Li, F., Wang, Y., Wang, Y., Ou, G., Cheng, S., Guan, S., Jia, M., Wu, L., Ding, X., and Xie, G. (2025). Hierarchical Co@C catalysts derived from metal-organic frameworks with tailored particle sizes for enhanced MgH_2 hydrogen storage. J. Energy Storage *138*, 118763.
26. Lv, M.-L., Zheng, J.-G., Xia, A., Zhang, Q.-B., Ma, Z.-X., Su, C., and Ge, L. (2025). Bimetallic Ti_2NbC_2 MXene as an efficient catalyst for reversible hydrogen storage in magnesium hydride. Rare Met. *44*, 2489–2501.
27. Zeng, L., Lan, Z., Li, B., Liang, H., Wen, X., Huang, X., Tan, J., Liu, H., Zhou, W., and Guo, J. (2022). Facile synthesis of a Ni_3S_2@C composite using cation exchange resin as an efficient catalyst to improve the kinetic properties of MgH_2. J. Magnes. Alloy. *10*, 3628–3640.
28. Yuan, Z., Li, S., Wang, K., Xu, N., Sun, W., Sun, L., Cao, H., Lin, H., Zhu, Y., and Zhang, Y. (2022). In-situ formed Pt nano-clusters serving as destabilization-catalysis bi-functional additive for MgH_2. Chem. Eng. J. *435*, 135050.
29. Zhang, L., Wang, K., Liu, Y., Zhang, X., Hu, J., Gao, M., and Pan, H. (2021). Highly active multivalent multielement catalysts derived from hierarchical porous $TiNb_2O_7$ nanospheres for the reversible hydrogen storage of MgH_2. Nano Res. *14*, 148–156.
30. Wan, H., Yang, X., Zhou, S., Ran, L., Lu, Y., Chen, Y., Wang, J., and Pan, F. (2023). Enhancing hydrogen storage properties of MgH_2 using FeCoNiCrMn high entropy alloy catalysts. J. Mater. Sci. Technol. *149*, 88–98.
31. Du, A.J., Smith, S.C., Yao, X.D., and Lu, G.Q. (2006). Ab initio studies of hydrogen desorption from low index magnesium hydride surface. Surf. Sci. *600*, 1854–1859.
32. Chen, W.-Y., Tang, J.-J., Lu, Z.-W., Huang, M.-X., Liu, L., He, C.-C., and Zhao, Y.-J. (2021). Theoretical investigation of the surface orientation impact on the hydrogen vacancy formation of MgH_2. Surf. Sci. *710*, 121850.

33. Ren, L., Li, Y., Li, Z., Lin, X., Lu, C., Ding, W., and Zou, J. (2024). Boosting hydrogen storage performance of MgH_2 by oxygen vacancy-rich H-V_2O_5 nanosheet as an excited H-pump. Nano-Micro Lett. *16*, 160.

34. Zhang, J., Wang, W., Chen, X., Jin, J., Yan, X., and Huang, J. (2024). Single-atom Ni supported on TiO_2 for catalyzing hydrogen storage in MgH_2. J. Am. Chem. Soc. *146*, 10432–10442.

35. Xu, N., Wang, K., Zhu, Y., and Zhang, Y. (2023). PdNi biatomic clusters from metallene unlock record-low onset dehydrogenation temperature for bulk-MgH_2. Adv. Mater. *35*, 2303173.

36. Morrison, O., Uteva, E., Walker, G.S., Grant, D.M., and Ling, S. (2025). Long time scale molecular dynamics simulation of magnesium hydride dehydrogenation enabled by machine learning interatomic potentials. ACS Appl. Energy Mater. *8*, 492–502.

37. Jia, B., Zhang, J., Chen, X., Zhang, J., Han, B., Wang, W., Yan, X., Shui, J., and Huang, J. (2025). Electronic structure modulation of Nb_2O_5 by Ru single atoms enabling efficient hydrogen storage of magnesium hydrides. Angew. Chem. Int. Ed. *64*, e202511139.

38. Ding, Y., Tong, L., Liu, X., Liu, Y., and Zhao, Y. (2025). Artificial intelligence-driven innovations in hydrogen storage technology. Energy Environ. Mater. *8*, e70041.

39. Angeletti, A., Leoni, L., Massa, D., Pasquini, L., Papanikolaou, S., and Franchini, C. (2025). Hydrogen diffusion in magnesium using machine learning potentials: a comparative study. npj Comput. Mater. *11*, 85.

40. Li, Q., Yan, M., Xu, Y., Zhang, X.L., Lau, K.T., Sun, C., and Jia, B. (2021). Computational investigation of MgH_2/NbO_x for hydrogen storage. J. Phys. Chem. C *125*, 8862–8868.

41. Li, Q., Qiu, S., Wu, C., Lau, K.T., Sun, C., and Jia, B. (2021). Computational investigation of MgH_2/graphene heterojunctions for hydrogen storage. J. Phys. Chem. C *125*, 2357–2363.

42. Duan, C., Wang, H., Wang, X., Liu, Y., Wu, J., Hu, L., Liu, B., Huang, H., Wang, F., and Wu, Y. (2025). The TM single-atom catalytic system bidirectionally enhances the hydrogen absorption/desorption kinetics of Mg/MgH_2: An insight into the synergetic enhancement mechanism and underlying principle. J. Magnes. Alloy. *13*, 5624–5636.

43. Zhang, J., Xia, G., Guo, Z., and Zhou, D. (2017). Synergetic effects toward catalysis and confinement of magnesium hydride on modified graphene: A first-principles study. J. Phys. Chem. C *121*, 18401–18411.

44. Dong, S., Liu, H., Liu, X., Li, C., Gao, Z., Liu, B., Yang, W., and Wu, Y. (2023). Facile dehydrogenation of MgH_2 enabled by γ-graphyne based single-atom catalyst. J. Energy Storage *74*, 109484.

45. Kuganathan, N., Dornheim, M., Grant, D.M., and Ling, S. (2025). Enhancing destabilization of MgH_2 with reactive elemental additives. J. Energy Storage *133*, 117959.

46. Fu, W., Shu, M., Liu, Y., Shi, J., Xu, Z., Yao, T., Liu, X., Dong, S., Gao, Z., and Yang, W. (2025). Unveiling the micro-mechanism of superior dehydrogenation in γ-MgH_2: Insights into the electronic structure of H–Mg bond. J. Alloys Compd. *1036*, 182130.

47. Dong, S., Li, C., Lv, E., Wang, J., Liu, H., Gao, Z., Xiong, W., Ding, Z., Yang, W., and Li, H. (2022). MgH_2/single-atom heterojunctions: effective hydrogen storage materials with facile dehydrogenation. J. Mater. Chem. A *10*, 19839–19851.

48. Jang, S.-H., Zhang, D., Tran, H.B., Jia, X., Konno, K., Sato, R., Orimo, S.-i., and Li, H. (2025). Physically interpretable descriptors drive the materials design of metal hydrides for hydrogen storage. Chem. Sci. *16*, 23111–23120.

49. Zhang, D., Jia, X., Tran, H.B., Jang, S.H., Zhang, L., Sato, R., Hashimoto, Y., Sato, T., Konno, K., Orimo, S.I., and Li, H. (2026). "DIVE" into hydrogen storage materials discovery with AI agents. Chem. Sci. *17*, 3031–3042.

50. Yao, T., Yang, Y., Cai, J., Liu, R., Dong, Z., Tang, X., Shao, X., Gao, Z., An, G., and Yang, W. (2026). From LLM to Agent: A large-language-model-driven machine learning framework for catalyst design of MgH_2 dehydrogenation. J. Magnes. Alloy. *14*, 101858. https://doi.org/10.1016/j.jma.2025.08.021.

51. Li, Y., Ren, L., Yao, Y., Zhao, Y., Xu, H., Li, Z., Li, Z., Dai, X., Tian, Y., Cao, S., et al. (2025). A single-atom interface engineering strategy to promote hydrogen sorption performances of magnesium hydride. Adv. Funct. Mater. *35*, 2417915.

52. Osman, A.I., Abd-Elaziem, W., Nasr, M., Farghali, M., Rashwan, A.K., Hamada, A., Wang, Y.M., Darwish, M.A., Sebaey, T.A., Khatab, A., and Elsheikh, A.H. (2024). Enhanced hydrogen storage efficiency with sorbents and machine learning: a review. Environ. Chem. Lett. *22*, 1703–1740.

53. Osman, A.I., Nasr, M., Mohamed, A.R., Abdelhaleem, A., Ayati, A., Farghali, M., Al-Muhtaseb, A.H., Al-Fatesh, A.S., and Rooney, D.W. (2024). Life cycle assessment of hydrogen production, storage, and utilization toward sustainability. WIREs Energy Environ *13*, e526.

54. Fu, W., Li, Y., Dong, Z., Li, J., Liu, R., Yang, Y., Li, J., Zhang, L., Wang, C., Yao, T., et al. (2026). Digital Hydrogen-S: An open-access interactive Data platform for solid-state hydrogen storage materials. Int. J. Hydrogen Energy *207*, 153434.

55. Yang, W., Xu, Z., Li, J., Zhang, L., Shu, M., Cai, J., Yao, T., Tang, X., Liu, Y., Luo, S., et al. (2026). XPEAK: an XRD-driven machine learning platform for predicting the catalyst-enhanced dehydrogenation peak temperature of MgH_2. J. Mater. Chem. A *14*, 7579–7595.

56. Ley, M.B., Jepsen, L.H., Lee, Y.-S., Cho, Y.W., Bellosta von Colbe, J.M., Dornheim, M., Rokni, M., Jensen, J.O., Sloth, M., Filinchuk, Y., et al. (2014). Complex hydrides for hydrogen storage - new perspectives. Mater. Today *17*, 122–128.

57. Sato, R., Conway, L.J., Zhang, D., Pickard, C.J., Akagi, K., Sau, K., Li, H., and Orimo, S.-I. (2025). Surface melting–driven hydrogen absorption for high-pressure polyhydride synthesis. Proc. Natl. Acad. Sci. USA *122*, e2413480122.